Editors' Suggestion

Cluster Frustration in the Breathing Pyrochlore Magnet $LiGaCr_4S_8$

Ganesh Pokharel,[1,2,*] Hasitha Suriya Arachchige,[1,2] Travis J. Williams,[3] Andrew F. May,[2] Randy S. Fishman,[2] Gabriele Sala,[3] Stuart Calder,[3] Georg Ehlers,[4] David S. Parker,[2] Tao Hong,[3] Andrew Wildes,[5] David Mandrus,[6,2,1] Joseph A. M. Paddison,[2,†] and Andrew D. Christianson[2,‡]

[1]*Department of Physics & Astronomy, University of Tennessee, Knoxville, Tennessee 37996, USA*
[2]*Materials Science & Technology Division, Oak Ridge National Laboratory, Oak Ridge, Tennessee 37831, USA*
[3]*Neutron Scattering Division, Oak Ridge National Laboratory, Oak Ridge, Tennessee 37831, USA*
[4]*Neutron Technologies Division, Oak Ridge National Laboratory, Oak Ridge, Tennessee 37831, USA*
[5]*Institut Laue-Langevin, CS 20156, 38042 Grenoble Cédex 9, France*
[6]*Department of Materials Science & Engineering, University of Tennessee, Knoxville, Tennessee 37996, USA*

(Received 21 February 2020; accepted 31 August 2020; published 16 October 2020)

We present a comprehensive neutron scattering study of the breathing pyrochlore magnet $LiGaCr_4S_8$. We observe an unconventional magnetic excitation spectrum with a separation of high- and low-energy spin dynamics in the correlated paramagnetic regime above a spin-freezing transition at 12(2) K. By fitting to magnetic diffuse-scattering data, we parametrize the spin Hamiltonian. We find that interactions are ferromagnetic within the large and small tetrahedra of the breathing pyrochlore lattice, but antiferromagnetic further-neighbor interactions are also essential to explain our data, in qualitative agreement with density-functional-theory predictions [Ghosh *et al.*, npj Quantum Mater. **4**, 63 (2019)]. We explain the origin of geometrical frustration in $LiGaCr_4S_8$ in terms of net antiferromagnetic coupling between emergent tetrahedral spin clusters that occupy a face-centered-cubic lattice. Our results provide insight into the emergence of frustration in the presence of strong further-neighbor couplings, and a blueprint for the determination of magnetic interactions in classical spin liquids.

DOI: 10.1103/PhysRevLett.125.167201

Geometrical frustration—the inability to satisfy all interactions simultaneously due to geometrical constraints—can generate unusual magnetic states in which long-range magnetic ordering is suppressed but strong short-range spin correlations endure [1]. Canonical models of frustrated magnetism often consider spins coupled by antiferromagnetic nearest-neighbor (NN) interactions, which generate a macroscopic degeneracy of magnetic ground states on lattices such as the pyrochlore network of corner-sharing tetrahedra [2–4]. This ground-state degeneracy is not symmetry protected, and in general is expected to be broken by perturbations such as further-neighbor interactions or spin-lattice coupling. Remarkably, however, some materials exhibit highly frustrated behavior, despite having complex magnetic interactions that deviate strongly from canonical frustrated models [5–7]. These states are of fundamental interest because they can reveal novel frustration mechanisms.

A modification of the pyrochlore lattice with the potential to realize such states is an alternating array of small and large tetrahedra [Fig. 1(a)]. This lattice is conventionally called a "breathing pyrochlore," although the size alternation is static and corresponds to a symmetry lowering from $Fd\bar{3}m$ to $F\bar{4}3m$ [8]. Different exchange interactions can occur within the small and large tetrahedra [J and J', respectively; see Fig. 1(a)], increasing the richness of the phase diagram [9]. Neglecting further-neighbor interactions, conventional ordering is expected only if both J and J' are ferromagnetic. If J and J' are both antiferromagnetic, the ground state is a classical spin liquid, whereas if J and J' are of opposite sign, the ground-state manifold is dimensionally reduced [9]. Further-neighbor interactions [J_2, J_{3a}, and J_{3b}; see Fig. 1(a)] can generate

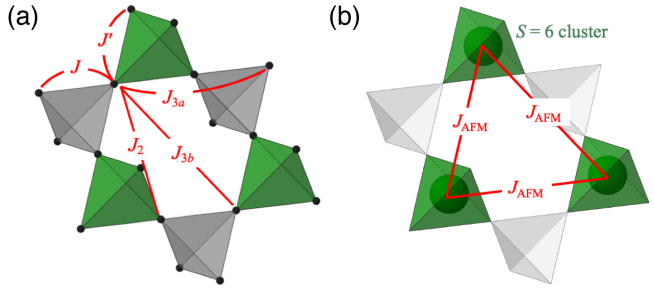

FIG. 1. (a) Breathing pyrochlore lattice of $S = 3/2$ Cr^{3+} ions (black circles) in $LiGaCr_4S_8$, showing large (small) tetrahedra [colored green (gray)], and the connectivity of the exchange interactions J, J', J_2, J_{3a}, and J_{3b}. J_{3a} and J_{3b} span the same distance but have different symmetry. (b) Emergent tetrahedral clusters generated by strong ferromagnetic J' interactions, coupled by a net antiferromagnetic interaction $J_{\mathrm{AFM}} \propto J + 4J_2 + 2J_{3a} + 2J_{3b}$ (> 0).

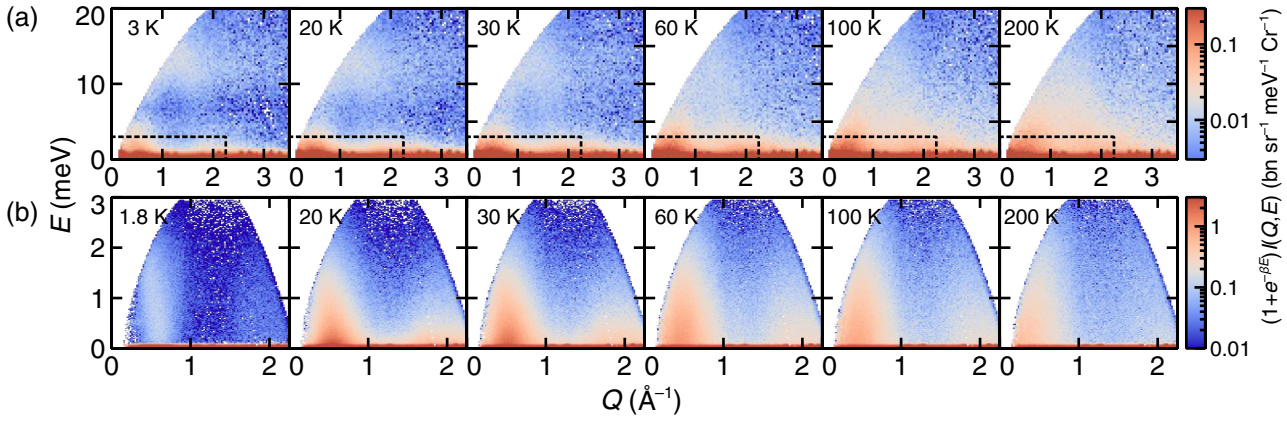

FIG. 2. Inelastic neutron scattering spectra of $LiGaCr_4S_8$ measured at temperatures indicated in the panels. (a) High-energy excitation spectra measured with $E_i = 25$ meV. (b) Low-energy spin excitations measured with $E_i = 3.32$ meV. The regions of the Q-E space enclosed by dotted lines in (a) indicate the regions shown in (b). Intensity is corrected for detailed balance and shown by color on a logarithmic scale. The intensity scale in (b) is a factor of 10 larger than in (a).

further exotic phases. Perhaps the most intriguing of these is predicted [10] to occur when J or J' is large and ferromagnetic and further-neighbor interactions are antiferromagnetic. The dominant ferromagnetic interactions drive the formation of ferromagnetic tetrahedral clusters, and intercluster interactions are frustrated because these clusters occupy a face-centered-cubic (fcc) lattice [Fig. 1(b)] [10]. This model provides a notable example of the concept of emergent frustration—the frustration of multispin degrees of freedom that occupy a different lattice to the spins themselves [6,7].

Experimental realizations of the breathing pyrochlore model include the spinel derivatives $AA'Cr_4X_8$, in which the A site is occupied by an ordered arrangement of Li^+ and In^{3+}/Ga^{3+}, X = O, S, or Se, and the Cr^{3+} ions occupy a breathing pyrochlore lattice [8]. Since $J \sim J'$ in these materials, collective magnetic behavior is expected, in contrast to the breathing pyrochlore material $Ba_3Yb_2Zn_5O_{11}$ in which tetrahedra are decoupled [11–15]. Series members with X = O have antiferromagnetic J and J' and exhibit magnetostructural phase transitions and nematic spin ordering [8,16–19]. Replacement of O with S or Se ligands is predicted to cause two key differences: suppression of direct exchange relative to superexchange, which is expected to be ferromagnetic because the Cr—X—Cr bond angles are near 90° [20], and enhancement of further-neighbor interactions [10]. Hence, series members with S or Se ligands [20–24] are promising candidates to realize models of frustration driven by further-neighbor interactions. However, no experimental determination of the magnetic interactions in such systems exists.

Here, we use neutron scattering measurements to study the breathing pyrochlore $LiGaCr_4S_8$. While the Weiss constant of $LiGaCr_4S_8$ is relatively small, $\theta_{CW} \approx 20$ K [20,23,25], its bulk magnetic susceptibility χ shows strong deviations from Curie-Weiss behavior below ~100 K, suggesting the development of strong spin correlations above its spin-freezing transition at $T_f = 12(2)$ K [20]. Spin freezing is probably driven by a small amount of off-stoichiometry, as approximately 4% of Li sites are occupied by Ga [20]. Our three key results explain the nature and origin of spin correlations in $LiGaCr_4S_8$: We experimentally parametrize the spin Hamiltonian to reveal the importance of further-neighbor couplings, we confirm recent theoretical predictions (Ref. [10]) of cluster frustration, and we observe a direct signature of cluster formation in its magnetic excitation spectrum. These results show that $LiGaCr_4S_8$ realizes the frustration of tetrahedral clusters on an emergent fcc lattice.

Figure 2 presents the temperature dependence of our inelastic neutron scattering (INS) data as a function of the wave vector transfer $Q = |\mathbf{Q}|$ and energy transfer E. Data were collected on a polycrystalline sample of mass ~2 g (see Supplemental Material [26]) using two neutron spectrometers: Fig. 2(a) shows high-energy data measured using the ARCS spectrometer with incident energy $E_i = 25$ meV, and Fig. 2(b) shows low-energy data measured using the CNCS spectrometer with $E_i = 3.32$ meV. All INS data have been corrected for detailed balance, and CNCS data are background subtracted. The dependence of the scattering on Q and temperature suggests that it is of magnetic origin.

The maximum magnetic excitation energy is about 15 meV, which is larger than the net interaction energy $\theta_{CW} \approx 20$ K (2 meV), suggesting that ferromagnetic and antiferromagnetic exchange interactions compete. Above 100 K the spectrum is broad, as expected for a paramagnet. In contrast, between 20 and 100 K, a band at ~12 meV and low-energy quasielastic excitations are observed. The low-energy scattering is much more intense than the high-energy scattering and has a pronounced wave vector dependence. On cooling, the quasielastic scattering moves toward low energy; however, analysis of the dynamical

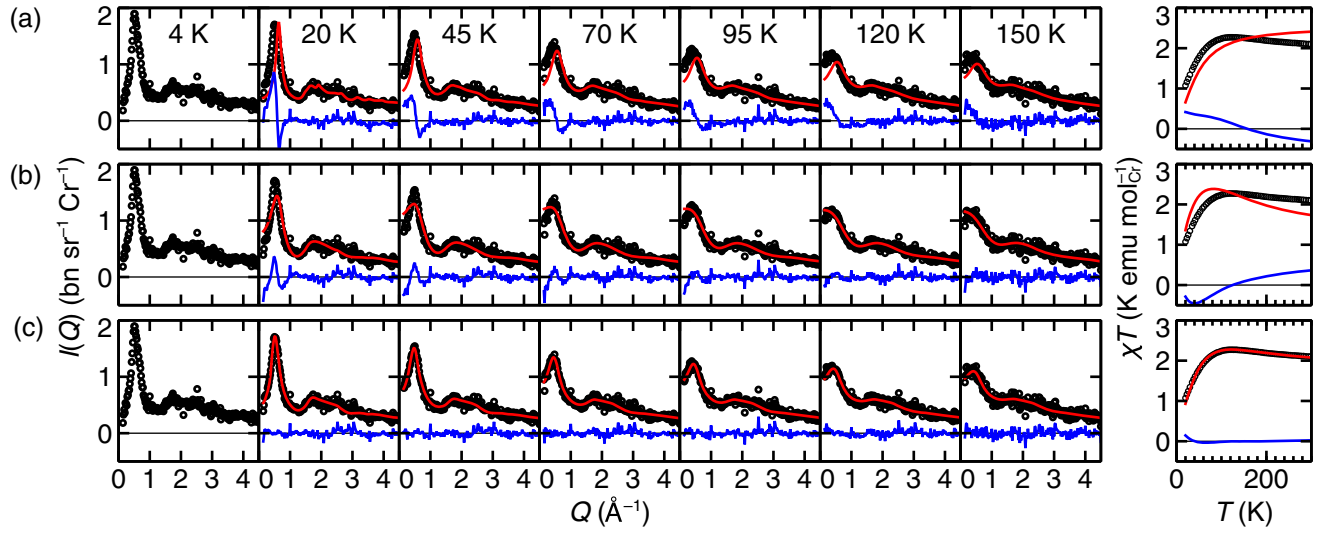

FIG. 3. Data (black circles), model fits (red lines), and data–fit (blue lines) for (a) the density-functional-theory (DFT) model of Ref. [10], (b) the J-J' model, and (c) the J-J'-J_2-J_{3a}-J_{3b} model discussed in the text. The left-hand panels of (a)–(c) represent the neutron scattering data at temperatures indicated in each panel, and the right-hand panel represents χ. Fits were performed for $T \geq 20$ K.

susceptibility using a damped-harmonic-oscillator model indicates that the excitations are overdamped and gapless at all measured temperatures [26]. Below T_f, most of the quasielastic spectral weight shifts to the elastic line [26], consistent with the expected dramatic slowing-down of spin dynamics associated with spin freezing [45]. Interestingly, the intensity of the high-energy band does not change appreciably compared to 20 K—a point to which we return below. Additional evidence of spin freezing is provided by our muon spin relaxation (μSR) measurements (see Supplemental Material [26]). Zero-field μSR measurements down to 1.8 K showed no evidence of static magnetic order or a canonical spin-glass state; however, the relaxation rate increased at the same temperature as seen with neutron scattering, suggesting a slowing-down of the spin fluctuations toward a frozen magnetic state. Longitudinal-field μSR does not show evidence of dynamic spin fluctuations, but rather agrees with the emergence of spin freezing at low temperature in $LiGaCr_4S_8$.

We now obtain an estimate of the magnetic interactions in $LiGaCr_4S_8$. Our starting point is a Heisenberg spin Hamiltonian $H = \frac{1}{2}\sum_{i,j} J_{ij}\mathbf{S}_i \cdot \mathbf{S}_j$, which has been applied successfully to Cr^{3+}-based spinels [46,47]. Here, $J_{ij} \in \{J, J', J_2, J_{3a}, J_{3b}\}$ denotes an interaction as shown in Fig. 1, and $\mathbf{S}$ denotes a classical vector of magnitude $\sqrt{S(S+1)}$ with $S = 3/2$. Our calculations assume Heisenberg spins on the breathing pyrochlore lattice and neglect chemical disorder. Because $LiGaCr_4S_8$ does not exhibit long-range magnetic order, it is not possible to employ the conventional approach of fitting interactions to spin-wave spectra in an ordered state. Therefore, we consider instead the magnetic diffuse-scattering intensity $I(Q) = \int I(Q, E)dE$, which we obtain from background-corrected powder-diffraction data collected using the HB-2A diffractometer at ORNL (see Supplemental Material [26]). For a given set of interaction parameters, we calculate $I(Q)$ and χT using Onsager reaction field theory [48–50], which is equivalent to the self-consistent Gaussian approximation used elsewhere [9,46,51] and gives accurate results for frustrated Heisenberg pyrochlore models [52].

We tested three models against our $I(Q)$ data and the χT data from Ref. [20] (Fig. 3). Values of the interaction parameters for each model are given in Table I. First, we considered the five-parameter "DFT model" obtained using the density-functional theory (DFT) in Ref. [10]. Calculations of $I(Q)$ and χT for this model show partial agreement with experiment; however, the calculated position of the main diffuse-scattering peak disagrees with the data [Fig. 3(a)]. Second, we fitted a simpler model to $I(Q)$ data that included J and J' interactions only ("J-J' model"). These fits also do not agree with the $I(Q)$ data and are inconsistent with the χT data [Fig. 3(b)]. Crucially, this result indicates that longer-ranged interactions beyond J and J' are essential to account for our experimental data. Finally, we fitted all five interaction parameters to our $I(Q)$ and χT data ("J-J'-J_2-J_{3a}-J_{3b} model"). Our data robustly determine a unique optimal solution (see Supplemental

TABLE I. Magnetic interaction parameters for different models. Parameter values held fixed are denoted by an asterisk (*).

Model	J (K)	J' (K)	J_2 (K)	J_{3a} (K)	J_{3b} (K)
DFT (Ref. [10])	−7.7(1)	−12.2(1)	1.2(1)	6.1(1)	3.0(1)
J-J'	3.07(3)	−29.9(4)	0*	0*	0*
J-J'-J_2-J_{3a}-J_{3b}	−7.8(6)	−22.1(3)	−1.6(4)	9.6(1)	0.8(4)

Material [26]) that gives a good fit to $I(Q)$ and χT at all temperatures [Fig. 3(c)]. We find J' is the largest interaction, J, J' are ferromagnetic, J_{3a} is antiferromagnetic, and J_2 and J_{3b} are small. The DFT model [10] shows the same trends. The consistency between the results derived by the two methods suggests that the trends determined by the modeling are physically reasonable. While it is not necessary to consider a possible temperature dependence of the interaction parameters [10] to model our data, a reduction in magnitude ~30% of J' and/or J on cooling from 150 to 20 K is not ruled out (see Supplemental Material [26]) and would be suitable for future theoretical investigation.

With an interaction model in hand, we consider the origin of frustration in $LiGaCr_4S_8$. We hypothesize that, at low temperature, spins coupled by dominant ferromagnetic J' are essentially aligned within the large tetrahedra, forming $S' \approx 6$ clusters. The lattice occupied by these clusters is fcc [Fig. 1(b)], and the net interaction between clusters for our parameters is given by $J_{\mathrm{AFM}} = (J + 4J_2 + 2J_{3a} + 2J_{3b})/16 = 0.43$ K [10]; i.e., it is antiferromagnetic. We therefore also hypothesize the suppression of T_f compared to J' occurs because of the frustration of antiferromagnetic intercluster interactions on the fcc lattice, as proposed theoretically in Ref. [10]. To test the hypothesis of ferromagnetic cluster formation, we performed classical Monte Carlo (MC) simulations driven by our fitted interaction parameters (see Supplemental Material [26]). Figure 4(a) shows that, at 20 K, the simulated spin-correlation function $\langle \mathbf{S}(0) \cdot \mathbf{S}(r) \rangle$ is close to unity at the distance r' within large tetrahedra, consistent with the MPDF [53] obtained by Fourier transforming our 20 K powder-diffraction data using $Q_{\mathrm{max}} = 2.5$ Å^{-1} to maximize the signal-to-noise ratio. This result shows that large tetrahedral clusters are essentially ferromagnetic at 20 K. Figure 4(b) shows the calculated temperature dependence of $\langle \mathbf{S}(0) \cdot \mathbf{S}(r = r') \rangle$, and reveals that the clusters are well established below 100 K. As described in the Supplemental Material [26], our own all-electron first-principles calculations support the ferromagnetic cluster picture presented here, along with the counterintuitive distance dependence of the exchange interactions. To test the hypothesis of antiferromagnetic frustration of $S' \approx 6$ cluster spins, we calculated the Fourier transform of the 3D spin-correlation function $I(\mathbf{Q}) \propto \sum_{\mathbf{r}} \langle \mathbf{S}(\mathbf{0}) \cdot \mathbf{S}(\mathbf{r}) \rangle \exp(i\mathbf{Q} \cdot \mathbf{r})$ from our Monte Carlo model using the program SCATTY [54]. Figure 4(c) shows the calculated $I(\mathbf{Q})$ for $LiGaCr_4S_8$ at 20 K. Figure 4(d) shows the calculated $I(\mathbf{Q})$ from the fcc lattice of cluster spins, defined on each tetrahedron of the breathing pyrochlore lattice as $\mathbf{S}' = \sum_{i=1}^{4} \mathbf{S}_i$. Figures 4(c) and 4(d) are different because the former includes the structure factor of the tetrahedral cluster, whereas the latter does not. Figure 4(e) shows the calculated $I(\mathbf{Q})$ for spins on the fcc lattice coupled by NN interactions J_{AFM}. The strong similarity between Figs. 4(d) and 4(e) demonstrates that antiferromagnetic interactions between cluster spins in $LiGaCr_4S_8$ are frustrated in the same way as individual spins on the fcc lattice.

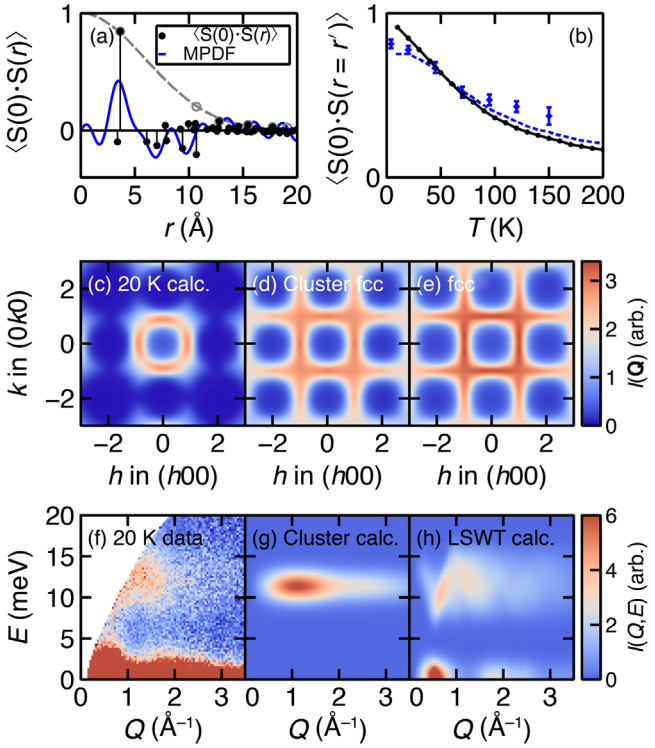

FIG. 4. (a) Spin correlations at 20 K as a function of distance r, showing $\langle \mathbf{S}(0) \cdot \mathbf{S}(r) \rangle$ from classical Monte Carlo (MC) simulations of our optimized interaction parameters (black bars and circles), and the magnetic pair-distribution function (MPDF) (blue line) [53]. The normalization is such that $\langle \mathbf{S}(0) \cdot \mathbf{S}(0) \rangle = 1$. The dashed gray line shows a fit of a Gaussian envelope to $\langle \mathbf{S}(0) \cdot \mathbf{S}(r) \rangle$, yielding spin correlation length $\sigma_r = 6.04(2)$ Å. (b) Temperature dependence of spin-spin correlators, showing MC results within large tetrahedra (black solid line), MC results summed over small and large tetrahedra (blue dotted line), and MPDF results integrated over small and large tetrahedra (blue circles). (c) Calculated single-crystal diffuse-scattering pattern $I(\mathbf{Q})$ in the $(hk0)$ plane at 20 K. (d) Calculated $I(\mathbf{Q})$ from the emergent fcc lattice of cluster spins defined as $\mathbf{S}' = \sum_{i=1}^{4} \mathbf{S}_i$ on each tetrahedron. (e) Calculated $I(\mathbf{Q})$ for spins on the fcc lattice with antiferromagnetic NN exchange interactions $J_{\mathrm{AFM}} = 0.43$ K. (f) Experimentally measured spin excitation spectrum at 20 K. (g) Calculated spin excitation spectrum of an isolated tetrahedral cluster. (h) Spin excitation spectrum calculated using linear spin wave theory (LSWT) assuming a proximate ordered ground state with propagation vector $\mathbf{k} = [0, 0, 1]$ [55].

The cluster model helps to explain our INS data. Our 20 K data are shown on a linear intensity scale in Fig. 4(f). To provide qualitative insight into these data, we show two approximate calculations that correspond to opposing limits. Figure 4(g) shows the excitation spectrum of an isolated tetrahedral cluster with internal ferromagnetic coupling J' [55,56]; its spectrum contains a single flat mode at $E = 4J'S$, whose intensity shows a broad peak

centered at a Q of approximately 1.1 Å^{-1}. Despite the simplicity of this calculation, it is in qualitative agreement with both the energy and wave vector dependence of the high-energy excitation in our INS data. Figure 4(h) shows the excitation spectrum of ferromagnetic tetrahedral clusters that are long-range ordered with wave vector $\mathbf{k} = [0, 0, 1]$ calculated using linear spin-wave theory around an assumed proximate ordered state using the SpinW software [55]. The former calculation neglects the effect of intertetrahedra coupling and consequently contains no low-energy excitations, whereas the latter overestimates the effect of intertetrahedra coupling. The spin-correlation length $\sigma_x = 6.04(2)$ Å at 20 K [Fig. 4(a)] exceeds the nearest-neighbor distance but is less than the cell parameter $a \approx 9.96$ Å, which suggests that the real material lies between these two limits (see Supplemental Material [26]).

Our results show that the origin of frustration in $LiGaCr_4S_8$ is the formation of tetrahedral clusters due to a dominant ferromagnetic J' interaction and the frustration of net antiferromagnetic intercluster interactions. This occurs because further-neighbor interactions are large, in agreement with DFT predictions [10] but in sharp contrast to oxide spinels [46]. We directly observe cluster formation via the development of an essentially intracluster high-energy mode in INS data. Such modes may potentially be present in other materials where emergent clusters are coupled by frustrated interactions, such as the metallic frustrated magnet β-$Mn_{0.8}Co_{0.2}$ [6] and the quantum-spin-liquid candidate $Ca_{10}Cr_7O_{28}$ [5]. In these cases, ferromagnetic interactions generate a triangular cluster lattice, in contrast to the fcc cluster lattice in $LiGaCr_4S_8$; however, a common feature is the higher symmetry of the emergent lattice compared to the parent lattice. Intriguingly, on traversing T_f, the high-energy mode in our INS data remains unchanged, whereas the low-energy excitations shift to the elastic line. Hence, the timescale of intercluster dynamics is enhanced below T_f, while that of the intracluster dynamics is unchanged. From the frequency dependence of ac susceptibility data [20], we obtain the Mydosh parameter $\delta T_f \sim 0.012$ (see Supplemental Material [26]). This value is an order of magnitude larger than that of canonical spin-glass systems such as AuMn [57] and CuMn [58], but is compatible with cluster-glass systems such as $Cr_{0.5}Fe_{0.5}Ga$ [59] and $Zn_3V_3O_8$ [60], suggesting that the ground state of $LiGaCr_4S_8$ is cluster-glass-like. It would therefore be interesting to investigate whether traditional cluster-glass materials—in which strong structural disorder typically generates clusters with a broad size distribution—exhibit distinct high-energy excitations similar to $LiGaCr_4S_8$. Our determination of the magnetic interactions of $LiGaCr_4S_8$ also sets a benchmark for quantitative interpretation of neutron data from polycrystalline samples. Our approach, while restricted to classical spins, can be generalized for different crystal structures, spin dimensionalities, and bond-dependent magnetic interactions [61].

We thank C. Batista for useful discussions and Gerald Morris for technical support with muon spin resonance measurements. This work was supported by the U.S. Department of Energy, Office of Science, Basic Energy Sciences, Materials Sciences and Engineering Division. G. P. and H. S. A. were partially supported by the Gordon and Betty Moore Foundation's EPiQS Initiative through Grant No. GBMF4416. J. A. M. P. acknowledges financial support from Churchill College, University of Cambridge, during early stages of this project. This research used resources at the Spallation Neutron Source and the High Flux Isotope Reactor, Department of Energy Office of Science User Facilities operated by Oak Ridge National Laboratory.

*gpokhare@vols.utk.edu
†paddisonja@ornl.gov
‡christiansad@ornl.gov

[1] L. Balents, Nature (London) **464**, 199 (2010).
[2] R. Moessner and J. T. Chalker, Phys. Rev. B **58**, 12049 (1998).
[3] R. Moessner and J. T. Chalker, Phys. Rev. Lett. **80**, 2929 (1998).
[4] B. Canals and C. Lacroix, Phys. Rev. Lett. **80**, 2933 (1998).
[5] C. Balz, B. Lake, J. Reuther, H. Luetkens, R. Schönemann, T. Herrmannsdörfer, Y. Singh, A. T. M. Nazmul Islam, E. M. Wheeler, J. A. Rodriguez-Rivera, T. Guidi, G. G. Simeoni, C. Baines, and H. Ryll, Nat. Phys. **12**, 942 (2016).
[6] J. A. M. Paddison, J. R. Stewart, P. Manuel, P. Courtois, G. J. McIntyre, B. D. Rainford, and A. L. Goodwin, Phys. Rev. Lett. **110**, 267207 (2013).
[7] J. W. F. Venderbos, M. Daghofer, J. van den Brink, and S. Kumar, Phys. Rev. Lett. **107**, 076405 (2011).
[8] Y. Okamoto, G. J. Nilsen, J. P. Attfield, and Z. Hiroi, Phys. Rev. Lett. **110**, 097203 (2013).
[9] O. Benton and N. Shannon, J. Phys. Soc. Jpn. **84**, 104710 (2015).
[10] P. Ghosh, Y. Iqbal, T. Müller, R. T. Ponnaganti, R. Thomale, R. Narayanan, J. Reuther, M. J. P. Gingras, and H. O. Jeschke, npj Quantum Mater. **4**, 63 (2019).
[11] K. Kimura, S. Nakatsuji, and T. Kimura, Phys. Rev. B **90**, 060414(R) (2014).
[12] T. Haku, K. Kimura, Y. Matsumoto, M. Soda, M. Sera, D. Yu, R. A. Mole, T. Takeuchi, S. Nakatsuji, Y. Kono, T. Sakakibara, L.-J. Chang, and T. Masuda, Phys. Rev. B **93**, 220407(R) (2016).
[13] J. G. Rau, L. S. Wu, A. F. May, A. E. Taylor, I.-L. Liu, J. Higgins, N. P. Butch, K. A. Ross, H. S. Nair, M. D. Lumsden, M. J. P. Gingras, and A. D. Christianson, J. Phys. Condens. Matter **30**, 455801 (2018).
[14] J. G. Rau, L. S. Wu, A. F. May, L. Poudel, B. Winn, V. O. Garlea, A. Huq, P. Whitfield, A. E. Taylor, M. D. Lumsden, M. J. P. Gingras, and A. D. Christianson, Phys. Rev. Lett. **116**, 257204 (2016).

[15] S.-Y. Park, S.-H. Do, K.-Y. Choi, J.-H. Kang, D. Jang, B. Schmidt, M. Brando, B.-H. Kim, D.-H. Kim, N. P. Butch, S. Lee, J.-H. Park, and S. Ji, Nat. Commun. **7**, 12912 (2016).

[16] Y. Okamoto, G. J. Nilsen, T. Nakazono, and Z. Hiroi, J. Phys. Soc. Jpn. **84**, 043707 (2015).

[17] S. Lee, S.-H. Do, W.-J. Lee, Y. S. Choi, M. Lee, E. S. Choi, A. P. Reyes, P. L. Kuhns, A. Ozarowski, and K.-Y. Choi, Phys. Rev. B **93**, 174402 (2016).

[18] R. Wawrzyńczak, Y. Tanaka, M. Yoshida, Y. Okamoto, P. Manuel, N. Casati, Z. Hiroi, M. Takigawa, and G. J. Nilsen, Phys. Rev. Lett. **119**, 087201 (2017).

[19] Y. Tanaka, R. Wawrzyńczak, M. D. Le, T. Guidi, Y. Okamoto, T. Yajima, Z. Hiroi, M. Takigawa, and G. J. Nilsen, J. Phys. Soc. Jpn. **87**, 073710 (2018).

[20] G. Pokharel, A. F. May, D. S. Parker, S. Calder, G. Ehlers, A. Huq, S. A. J. Kimber, H. S. Arachchige, L. Poudel, M. A. McGuire, D. Mandrus, and A. D. Christianson, Phys. Rev. B **97**, 134117 (2018).

[21] R. Plumier, F. Lotgering, and R. Van Stapele, J. Phys. (Paris), Colloq. **32**, C1-324 (1971).

[22] R. Plumier, M. Sougi, and M. Lecomte, Phys. Lett. **60A**, 341 (1977).

[23] Y. Okamoto, M. Mori, N. Katayama, A. Miyake, M. Tokunaga, A. Matsuo, K. Kindo, and K. Takenaka, J. Phys. Soc. Jpn. **87**, 034709 (2018).

[24] H. Duda, E. Maciazek, T. Gron, S. Mazur, A. W. Pacyna, A. Waskowska, T. Mydlarz, and A. Gilewski, Phys. Rev. B **77**, 035207 (2008).

[25] H. Pinch, M. Woods, and E. Lopatin, Mater. Res. Bull. **5**, 425 (1970).

[26] See Supplemental Material at http://link.aps.org/supplemental/10.1103/PhysRevLett.125.167201 for additional experimental details, low energy neutron scattering results and analysis, muon spin resonance results, diffuse scattering analysis, and first principles calculations (see also Refs. [27–44] therein).

[27] J. Rodriguez-Carvajal, Physica **55B**, 192 (1993).

[28] D. L. Abernathy, M. B. Stone, M. J. Loguillo, M. S. Lucas, O. Delaire, X. Tang, J. Y. Y. Lin, and B. Fultz, Rev. Sci. Instrum. **83**, 015114 (2012).

[29] G. Ehlers, A. A. Podlesnyak, J. L. Niedziela, E. B. Iverson, and P. E. Sokol, Rev. Sci. Instrum. **82**, 085108 (2011).

[30] O. Arnold *et al.*, Nucl. Instrum. Methods Phys. Res., Sect. A **764**, 156 (2014).

[31] R. T. Azuah, L. R. Kneller, Y. Qiu, P. L. W. Tregenna-Piggott, C. M. Brown, J. R. D. Copley, and R. M. Dimeo, J. Res. Natl. Inst. Stand. Technol. **114**, 341 (2009).

[32] G. J. Nilsen, Y. Okamoto, T. Masuda, J. Rodriguez-Carvajal, H. Mutka, T. Hansen, and Z. Hiroi, Phys. Rev. B **91**, 174435 (2015).

[33] S.-H. Lee, J. M. Tranquada, K. Yamada, D. J. Buttrey, Q. Li, and S.-W. Cheong, Phys. Rev. Lett. **88**, 126401 (2002).

[34] Y. Y. Peng, E. W. Huang, R. Fumagalli, M. Minola, Y. Wang, X. Sun, Y. Ding, K. Kummer, X. J. Zhou, N. B. Brookes, B. Moritz, L. Braicovich, T. P. Devereaux, and G. Ghiringhelli, Phys. Rev. B **98**, 144507 (2018).

[35] P. H. Conlon and J. T. Chalker, Phys. Rev. Lett. **102**, 237206 (2009).

[36] B. S. Garbow, Comput. Phys. Commun. **7**, 179 (1974).

[37] P. J. Brown, *International Tables for Crystallography* (Kluwer Academic Publishers, Dordrecht, 2004), pp. 454–460.

[38] M. Enjalran and M. J. P. Gingras, Phys. Rev. B **70**, 174426 (2004).

[39] F. James and M. Roos, Comput. Phys. Commun. **10**, 343 (1975).

[40] J. P. Perdew, K. Burke, and M. Ernzerhof, Phys. Rev. Lett. **77**, 3865 (1996).

[41] P. Blaha, K. Schwarz, G. K. H. Madsen, D. Kvasnicka, and J. Luitz, WIEN2K, *An Augmented Plane Wave+Local Orbitals Program for Calculating Crystal Properties* (Vienna University of Technology, Vienna, 2017).

[42] T. J. Williams, A. E. Taylor, A. D. Christianson, S. E. Hahn, R. S. Fishman, D. S. Parker, M. A. McGuire, B. C. Sales, and M. D. Lumsden, Appl. Phys. Lett. **108**, 192403 (2016).

[43] K. V. Shanavas, D. Parker, and D. J. Singh, Sci. Rep. **4**, 7222 (2014).

[44] M. A. McGuire, H. Cao, B. C. Chakoumakos, and B. C. Sales, Phys. Rev. B **90**, 174425 (2014).

[45] K. Binder and A. P. Young, Rev. Mod. Phys. **58**, 801 (1986).

[46] X. Bai, J. A. M. Paddison, E. Kapit, S. M. Koohpayeh, J.-J. Wen, S. E. Dutton, A. T. Savici, A. I. Kolesnikov, G. E. Granroth, C. L. Broholm, J. T. Chalker, and M. Mourigal, Phys. Rev. Lett. **122**, 097201 (2019).

[47] M. Matsuda, H. Ueda, A. Kikkawa, Y. Tanaka, K. Katsumata, Y. Narumi, T. Inami, Y. Ueda, and S.-H. Lee, Nat. Phys. **3**, 397 (2007).

[48] R. Brout and H. Thomas, Phys. Phys. Fiz. **3**, 317 (1967).

[49] D. E. Logan, Y. H. Szczech, and M. A. Tusch, Europhys. Lett. **30**, 307 (1995).

[50] D. Hohlwein, J.-U. Hoffmann, and R. Schneider, Phys. Rev. B **68**, 140408(R) (2003).

[51] K. W. Plumb, H. J. Changlani, A. Scheie, S. Zhang, J. W. Krizan, J. A. Rodriguez-Rivera, Y. Qiu, B. Winn, R. J. Cava, and C. L. Broholm, Nat. Phys. **15**, 54 (2019).

[52] P. H. Conlon and J. T. Chalker, Phys. Rev. B **81**, 224413 (2010).

[53] B. A. Frandsen, X. Yang, and S. J. L. Billinge, Acta Crystallogr. Sect. A **70**, 3 (2014).

[54] J. A. M. Paddison, Acta Crystallogr. Sect. A **75**, 14 (2019).

[55] S. Toth and B. Lake, J. Phys. Condens. Matter **27**, 166002 (2015).

[56] K. Prša and O. Waldmann, Inorganics **6** 49, (2018).

[57] C. A. M. Mulder, A. J. van Duyneveldt, and J. A. Mydosh, Phys. Rev. B **25**, 515 (1982).

[58] C. A. M. Mulder, A. J. Van Duyneveldt, and J. A. Mydosh, Phys. Rev. B **23**, 1384 (1981).

[59] P. Bag, P. R. Baral, and R. Nath, Phys. Rev. B **98**, 144436 (2018).

[60] T. Chakrabarty, A. V. Mahajan, and S. Kundu, J. Phys. Condens. Matter **26**, 405601 (2014).

[61] J. A. M. Paddison, arXiv:2002.12894.